geoconvention
Calgary • Canada • May 7-11 2018

Sonic tensor completion

Scott Leaney and Jeroen Jocker
Schlumberger

Summary

Sonic slowness measurements in a vertical well are augmented with auxiliary data to provide plausible logs of fractured vertical transverse isotropy (FVTI) moduli. The auxiliary data come from published core measurements, described by a mean vector containing five VTI parameters and an associated covariance matrix. A Bayesian formalism is used to bring in the auxiliary data. The inversion seeks an FVTI medium that fits the sonic measurements while honoring the data base, exploiting correlations between the in situ and auxiliary measurements. The data base is used to constrain VTI tensor components for the background medium as well as in both symmetry planes. A seven-parameter model vector $(V_P, V_S, E, A, G, \delta_N, \delta_V)$ is found through nonlinear optimization. Together with the sonic fast shear azimuth, a depth-dependent monoclinic medium can be constructed and upscaled to seismic frequencies. Applications include seismic simulation and background priors for orthorhombic tomography and AVA vs. azimuth inversion.

Introduction

Sonic slowness measurements in a vertical borehole provide four density-normalized stiffness moduli: $a33, a44, a55, a66$. High-frequency monopole waveforms provide the compressional slowness, crossed-dipole waveforms provide fast and slow shear slownesses from the flexural waves and low-frequency monopole waveforms provide a horizontal shear slowness from the Stoneley dispersion. In a medium with vertical fractures or horizontal stress anisotropy, $a44$ and $a55$ define a shear splitting parameter whereas in a VTI medium, $a66$ with $a44$ provide Thomsen's gamma parameter. Thus, sonic measurements in a vertical well measure part of a horizontal transverse isotropy (HTI) medium and part of a VTI medium. Missing are the horizontal compressional moduli, $a11$ and $a22$, and off-axis moduli, $a13$ and $a23$. We seek to determine the additional four moduli for a fractured VTI medium and, in completing the tensor, expand the usefulness of sonic anisotropy measurements.

Previous work to invert for a VTI tensor from sonic measurements made use of logs from multiple well deviations drilled through the same formation. Hornby et al. (2003) considered compressional slownesses and inverted for Thomsen's ε and δ. Miller et al. (2012) considered compressional and shear slownesses and inverted for a complete VTI tensor. Jocker et al. (2013) included a clustering approach to handle heterogeneity in an inversion of data from deviated boreholes. Sinha et al. (2014) proposed a linearized inversion of crossed-dipole flexural wave dispersion in a vertical well for four moduli; a simple linear correlation between $a33$ and $a11$ was then used to complete the VTI tensor. Recently, a Bayesian approach was developed to invert for VTI anisotropy from a single vertical or deviated well (Jocker, pers. comm., 2016). Here, we limit our scope to vertical wells but extend this technique to invert for a medium with lower symmetry than VTI.

Theory and Method

An FVTI medium is a simple class of orthorhombic medium requiring eight parameters for its representation. We follow Schoenberg and Helbig (1997) and construct the FVTI medium by adding compliant fractures to a background VTI medium. The fractures are described by dimensionless crack compliance parameters $(\delta_N, \delta_V, \delta_H)$ corresponding to normal and shear excess compliances. Using the

subscript "b" to signify the background medium, the FVTI moduli correponding to the sonic measurements are given as

$$a33 = a33_b\left(1 - \delta_N \frac{{a13_b}^2}{a11_b a33_b}\right),\ a44 = a44_b,\ a55 = a44_b(1 - \delta_V),\ a66 = a66_b(1 - \delta_H). \tag{1}$$

In practice, the background VTI medium is specified through anisotropy parameters, and the background moduli are backcalculated. The complete FVTI tensor is not written out here; please see equation (10) in Schoenberg and Helbig (1997).

The best-fit FVTI medium is parameterized using $(V_P, V_S, E, A, G, \delta_N, \delta_V, \delta_H)$. The background VTI parameters (E, A, G) are due to Schoenberg (Carrion et al., 1992, Schoenberg and de Hoop, 2000) and are used for inversion because they are bounded on $[-1, +1]$; they are analogous to Thomsen parameters $(\varepsilon, \sigma, \gamma)$. The 7-vector of model parameters is determined by minimizing an objective function, constructed with standard Bayesian log- likelihood and prior terms as

$$\Phi = \frac{\left(\boldsymbol{d} - \boldsymbol{d}(\boldsymbol{m})\right)^2}{\boldsymbol{\sigma}} + (\boldsymbol{m_b} - \widehat{\boldsymbol{m}})^T {\boldsymbol{C_m}}^{-1}(\boldsymbol{m_b} - \widehat{\boldsymbol{m}}) + \left(\boldsymbol{m_f} - \widehat{\boldsymbol{m}}\right)^T {\boldsymbol{C_m}}^{-1}\left(\boldsymbol{m_f} - \widehat{\boldsymbol{m}}\right) + (\boldsymbol{m_s} - \widehat{\boldsymbol{m}})^T {\boldsymbol{C_m}}^{-1}(\boldsymbol{m_s} - \widehat{\boldsymbol{m}}). \tag{2}$$

The data vector, $\boldsymbol{d}$, contains the four measured slownesses, and the modelled data, $\boldsymbol{d}(\boldsymbol{m})$, are the four axial FVTI moduli from equation (1) converted to slownesses. Data errors, $\boldsymbol{\sigma}$, come from sonic slowness processing and are on the order of a percent; the error is larger for Stoneley shear due to its dependence on an uncertain mud slowness, mobility and other effects. As always, care must be taken to quality-control sonic slowness processing. $\boldsymbol{m_b}$, $\boldsymbol{m_f}$ and $\boldsymbol{m_s}$ are the VTI parameter vectors for the background medium, fast-direction medium and slow-direction medium, respectively, extracted from the FVTI tensor. The prior model vector, $\widehat{\boldsymbol{m}}$, corresponds to the data base means, and $\boldsymbol{C_m}$ is the corresponding covariance matrix. Objective function (2) is minimized using the simplex algorithm due to Nelder and Mead (1965) (Press et al., 2004); posterior covariance is determined using Makov chain Monte Carlo (MCMC) sampling (e.g., Malinverno and Leaney, 2005).

The data base behind the Bayesian prior was assembled from 245 published core measurements of VTI anisotropy. From these, means and covariances were computed. Figure 1 shows the data base plotted on density-coloured multivariate normal samples for pairs of anisotropy parameters.

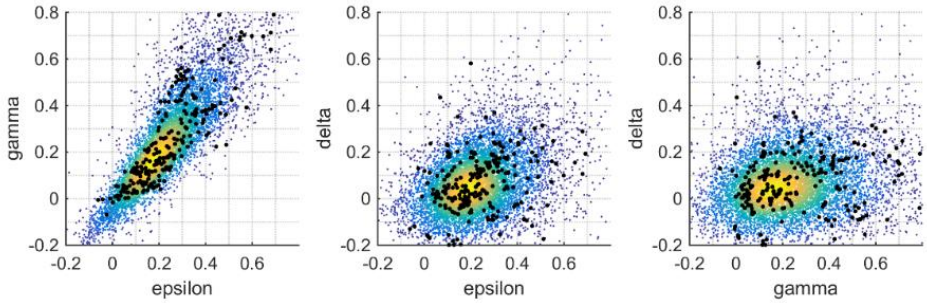

Figure 1. Data base samples (black dots) on top of multivariate normal samples using data base means and covariances. Only anisotropy parameters are shown; V_P and V_S are also in the data base.

The algorithm proceeds on a depth-by-depth basis. Because the inversion is nonlinear, initial guesses are needed. V_P and V_S are obtained from the compressional and fast shear slownesses; the S_H VTI parameter is obtained from Stoneley shear slowness and hence $a66$ to provide G from $G = (a66 - a44)/(a66 + a44)$. The compressional ellipticity parameter, E, and anellipticity, A, initial guesses are obtained from curvilinear data base correlations with G; thus, depths with larger G will start with larger E and A. δ_V is obtained from the fast and slow shear slownesses as $\delta_V = 1 - a55/a44$. The δ_N initial guess is obtained from δ_V given a user-defined value for compliance ratio Z_N/Z_V. δ_H is fixed given Z_H/Z_V.

Figure 2 shows the posterior for a given depth and the progress of the MCMC random walk algorithm towards the solution. Here, the initial guess was $(0,0)$ for (A, G), so, after a brief journey towards the solution, the MCMC algorithm samples around the solution to provide the posterior probability distribution. In practice, the initial guess discussed previously is better than $(0,0)$ and the simplex algorithm is more efficient at finding the optimum, so it is used. MCMC is then used to provide the posterior histograms. Also shown in Figure 2 are posterior histograms without data base information and with data base information. As expected, using measurements alone, only G and δ_V are resolved. When auxiliary data from the data base are incorporated, the remaining anisotropy parameters are resolved. Notice that the P ellipticity parameter in red has a narrower histogram than A and δ_N due to the strong correlation between E (ε) and G (γ), as seen in Figure 1 (left plot). To further explore the properties of the algorithm we now look at results over a section of reservoir sonic.

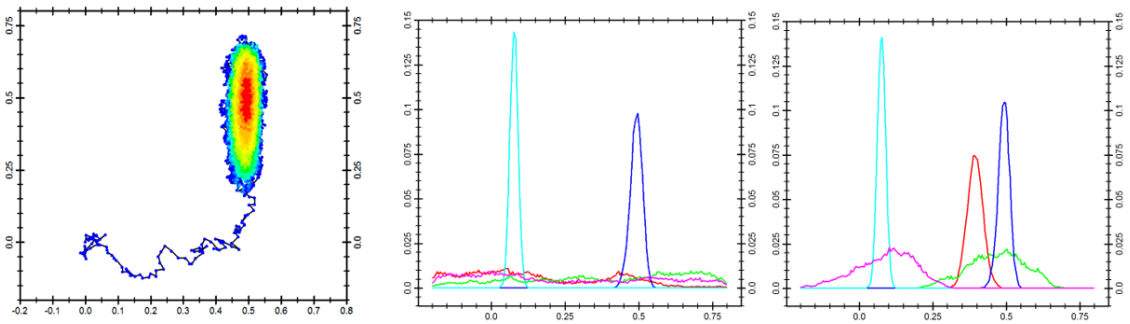

Figure 2. Left: Posterior for A vs. G through the random walk of the MCMC algorithm, starting from $(0,0)$. MCMC samples the posterior distribution allowing histograms to be computed. Middle: histograms for anisotropy parameters $(E, A, G, \delta_V, \delta_N)$=(red,green,blue,cyan,magenta) without data base constraint. Right: Same as middle but with data base constraint.

The field data set comes from a section over the Morrow sand in north Texas. Figure 3 shows posterior histograms for the five FVTI anisotropy parameters. Histograms for V_P and V_S are not shown. As expected, the measurements constrain G and δ_V. Their histogram widths come from the combination of slowness measurement errors. Background VTI parameters E and A are determined from data base correlation and their histograms come from the data base covariance. The anellipticity parameter, A, shows larger uncertainty because off-axis core measurements are difficult and error-prone, this is captured in the data base covariance matrix. The normal crack compliance parameter, δ_N, is poorly resolved. There is no measurement or data base covariance for this parameter; its resolution comes from the VTI constraints in symmetry planes while satisfying fast and slow shear measurements. The parameter δ_H is not resolved as it appears in the G VTI parameter in both fast and slow directions. In this example, there is strong VTI above and below the sandstone reservoir whereas within the reservoir, there is some HTI. There are also depths where both flavors of anisotropy are present, for example, below the base reservoir boundary.

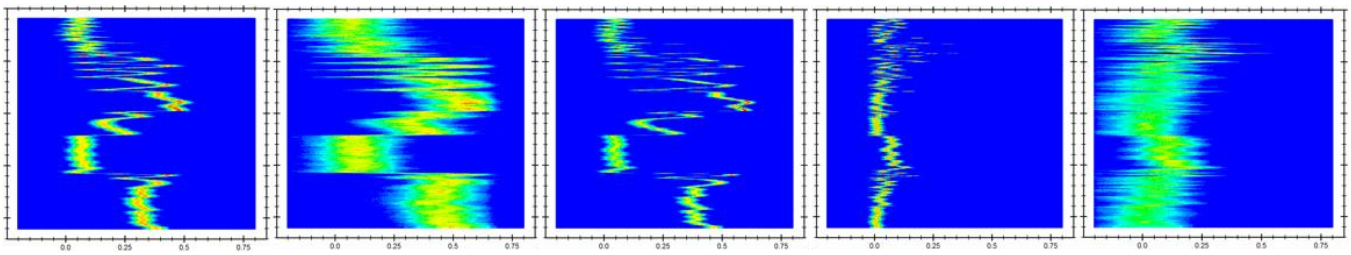

Figure 3. Depth-dependent histograms for the five FVTI anisotropy parameters. From left to right: $(E, A, G, \delta_V, \delta_N)$. Horizontal scale is $[-0.2, +0.8]$. G and δ_V are resolved by measurements; E, A and δ_N come from data base correlations.

Having determined the parameters of an FVTI medium at sonic scale, the moduli can be recast into any preferred parameterization, for example, that due to Tsvankin (1997). The orientation of the FVTI medium may come from the shear fast azimuth from crossed-dipole sonic logging. When the FVTI medium is rotated based on the fast shear azimuth angle using the modified Bond transform (Chapman, 2004), it becomes a monoclinic medium. To upscale a stack of such media, the method of Schoenberg and Muir (1989) is required, then ray tracing through monoclinic layers may be done. Figure 4 shows monoclinic P-p and P-sv AVA vs. azimuth for the base reservoir interface after upscaling. Another useful product from the FVTI logs is to determine the nearest VTI medium (e.g., Dellinger, 2005), or simply use the background VTI medium, which is the medium in the absence of fractures or horizontal stress anisotropy.

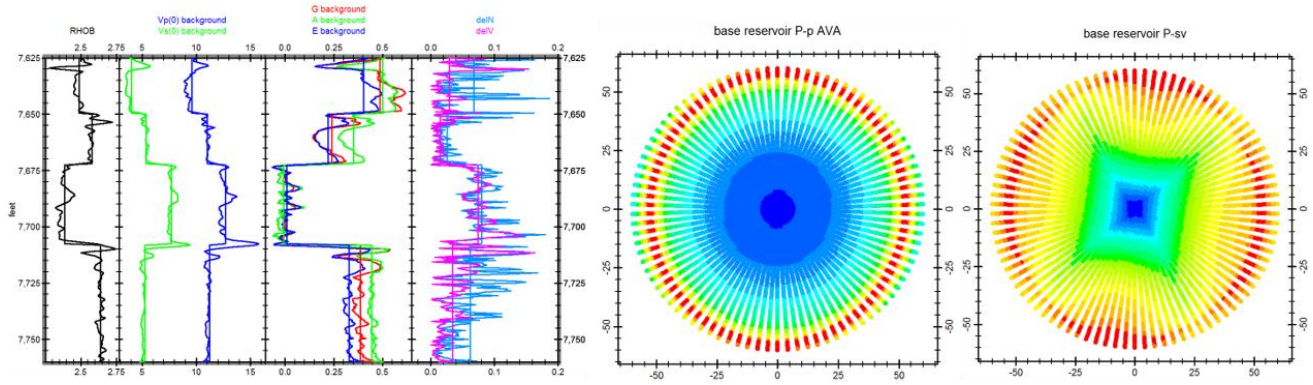

Figure 4. Left: sonic FVTI logs and upscaled averages. Middle and right: P-p and P-sv base reservoir AVA vs. azimuth. Maximum incidence phase angle is 60°, fast shear azimuth is N100E.

Conclusions

We described a technique to complete an FVTI stiffness tensor using vertical well sonic slownesses and an auxiliary data base. The in situ and auxiliary data were brought together in a Bayesian framework. Together with the fast shear azimuth, logs of monoclinic moduli can be produced; the nearest VTI medium is also a useful product. Completing the tensor expands the usefulness of sonic anisotropy measurements. We expect these completed elastic anisotropy logs to have many uses, for example, in seismic simulation and in constructing prior models for microseismic model calibration, orthorhombic tomography and AVA vs. azimuth inversion.

Acknowledgements

Thanks to Edan Gofer and Colin Sayers for great discussions. The field data in Figures 3 and 4 are related to work supported by the U.S. DOE National Energy Technology Laboratory under Award Number DE-FC26-05NT42591. Additional support has been provided by site operator Chaparral Energy, L.L.C.

References

Carrion, P., J. Costa, J.E Ferrer Pinheiro and M. Schoenberg, 1992, Cross-borehole tomography in anisotropic media: *Geophysics*, 57, 1194-1198.

Chapman, C.H., 2004, Fundamentals of seismic wave propagation, Cambridge University Press.

Dellinger, J., 2005, Computing the optimal transversely isotropic approximation of a general elastic tensor: *Geophysics*, 70, I1–I10.

Hornby, B. E., J. M. Howie and D. W. Ince, 2003, Anisotropy correction for deviated-well sonic logs: Application to seismic well tie: *Geophysics*, 68, 464–471.

Jocker, J., E. Wielemaker, S. Sunaga, M. Ferla and F. Pampuri, 2013, TI anisotropic model building using borehole sonic logs acquired in heterogeneous formations: *SEG Expanded Abstracts*, 305–309.

Malinverno, A., and W.S. Leaney, 2005, Monte-Carlo Bayesian look-ahead inversion of walkaway vertical seismic profiles: *Geophysical Prospecting*, **53**, 689–703.

Miller, D. E., S. A. Horne and J. Walsh, 2012, Precise inversion of logged slownesses for elastic parameters in a gas shale formation: *Geophysics*, **77**, no. 4, B197–B206.

Nelder, J. A., and R. Mead, 1965, A simplex method for function minimization: *Computer Journal*, **7**, 308–313.

Press, W., S. Teukolsky, W. Vetterling and B. Flannery, 2004, *Numerical Recipes in Fortran 77: The Art of Scientific Computing*, Cambridge University Press.

Schoenberg, M., and K. Helbig, 1997, Orthorhombic media: Modeling elastic wave behavior in a vertically fractured earth: *Geophysics*, **62**, 1954-1974.

Schoenberg, M., and M. V. de Hoop, 2000, Approximate dispersion relations for qP-qSV-waves in transeversely isotropic media: *Geophysics*, **65**, 919-953.

Schoenberg, M., and F. Muir, 1989, A calculus for finely layered anisotropic media: *Geophysics*, **54**, 581-589.

Sinha, B. K., A. Donald, J. Walsh and T. Lei, 2014, Anisotropic elastic constants from dipole flexural dispersion in unconventional shale-gas reservoirs: 84th Annual International Meeting, SEG, Expanded Abstracts.

Tsvankin, I., 1997, Anisotropic parameters and P-wave velocity for orthorhombic media: *Geophysics*, **62**, 1292–1309.